

# Reconstruction using surface dedicated tensorial fields

MARCELO BERNARDES VIEIRA<sup>1</sup>, MATTHIEU CORD<sup>3</sup>, PAULO P. MARTINS JR.<sup>4</sup>,  
SYLVIE PHILIPP-FOLIGUET<sup>3</sup>, ARNALDO DE A. ARAÚJO<sup>2</sup>

<sup>1</sup>IMPA - Instituto de Matemática Pura e Aplicada, Est. Dona Castorina, 110, 22460-320, Rio de Janeiro, RJ, Brazil  
mbvieira@impa.br

<sup>2</sup>NPDI/DCC - Universidade Federal de Minas Gerais, Caixa Postal 702, 30161-970, Belo Horizonte, MG, Brazil  
arnaldo@dcc.ufmg.br

<sup>3</sup>Ecole Nationale Supérieure d'Electronique et de ses Applications, 6 av. du Ponceau, 95014, Cergy Cedex, France  
{cord, philipp}@ensea.fr

<sup>4</sup>Centro Tecnológico de Minas Gerais, av. José Cândido da Silveira, 2000, 31170-000, Belo Horizonte, MG, Brazil  
pmartin@cetec.br

**Abstract.** We propose in this paper a new strategy to estimate surface normals from sparse data for reconstruction. Our approach is based on tensorial fields morphologically adapted to infer normals forming smooth surfaces. They act as three-dimensional structuring elements for finding precise normals. Robust orientation inference is performed by an enhanced accumulation process using the tensorial fields. The surface dedicated aspects of our propositions are suitable for smooth surface inference from noisy data. We present qualitative and quantitative results to show the behavior of the original methods and ours. A comparative discussion of these results remarks the efficiency of our extensions.

## 1 Introduction

Surface reconstruction concerns the problem of retrieving three-dimensional shapes which, in general, represent a physical object. In most cases, only points distributed over the object are known. Obtaining precise 3D models of real objects has applications in reverse engineering, shape analysis, computer graphics, computer vision, among others.

The most important works on surface reconstruction classify sparse data as an *unorganized point set* [1, 2]. In Gopi & Krishnan [3], a set of points is classified *organized* if it has additional information about the original surface.

However, we remark that any sparse set of points is at least assumed to be *implicitly organized* since the points, or a subset of them, are *structured* over an object. In our work, organized points are those that, within their neighborhood, are structured over a surface.

The spatial organization effectively allows the extraction of the original structuring object. However, surface reconstruction is a harder problem when information about the points organization is limited or missing. Precise normals associated to points, for example, make the reconstruction task easier.

Sparse data representing objects may have outliers and additive noise in real applications. In Gideon Guy's paradigm [4, 5], surface reconstruction is made by evaluating the sparse data organization. More precisely, Guy provides two functions  $\mathbf{n}(D, Q) \rightarrow \mathbb{R}^3$  and  $s(D, Q) \rightarrow \mathbb{R}^+$ , where  $D$  is a sparse data set and  $Q \in \mathbb{R}^3$  is an arbitrary point, in such a way that

- $\mathbf{n}(D, Q)$  is the estimation of a normal in  $Q$  representing a surface that presumably structures  $Q$  in conjunction with its neighborhood in  $D$ ;

- $s(D, Q)$  is the pertinence, or relevance degree of the normal estimate in comparison with the original object represented by  $D$ .

Set  $D$  may have points, points with associated normal (surfels) and points with associated tangent (curvels). Based on continuation constraints, Guy defined a three-dimensional field of tensors for each input class.

Using these fields, the structural contributions of each element are accumulated to infer normals  $\mathbf{n}(D, P)$  and pertinences  $s(D, P)$  for every  $P \in D$ . Next, the field for surfels is aligned with the inferred normal in every input point and the contributions are accumulated in the subspace containing  $D$ . Resulted tensors representing the subspace are decomposed and the surface and curves formed by the input points are retrieved by a local maxima extraction algorithm.

Lee & Medioni [6] extended Guy's method using orientation tensors [7]. The main difference is that fields and accumulation processes are based on tensor spectral decomposition rather than input classes. Curves formed by input points are retrieved using surface uncertainty obtained in tensors. This new approach gives better results than the original method but uncertainty propagation interferes on surface reconstruction.

Guy's method and its extensions are defined for surface and curve reconstruction in the same process. We ar-

gue that one may obtain much better results if the tensor coding, the tensorial fields morphology and the accumulation process are specific for the desired structure. In this paper, we present new tensorial fields and accumulation processes for surface reconstruction.

## 2 Method overview

Surface reconstruction is achieved in two steps (Fig. 1). Firstly, normals and associated pertinences are computed for every input element. We propose an enhancement method that gives better estimates due to the surface dedicated tensorial fields and accumulation process. It is also robust to additive noise and outliers.

In the second step, the contribution of each point is accumulated in subspace containing the input elements using the tensorial field for normals. This field is morphologically adapted to infer normals forming smooth surfaces. As in Guy's method, the final surface is obtained by local maxima extraction using resulting tensors.

Note that the second step is absolutely dependent of the information inferred in the first one. Thus, our enhancement process augments considerably the reconstruction result.

Tensorial fields are constructed with a suitable tensor coding and appropriated continuation constraints to obtain better normal estimates. See that indecision information about normals obtained in tensors is discarded in all steps.

We describe in Section 3 the fields and the accumulation process for finding enhanced normal vectors. The dense accumulation for surface reconstruction is presented in Section 4. In Section 5, we show some experimental quantitative and qualitative results for comparison purposes.

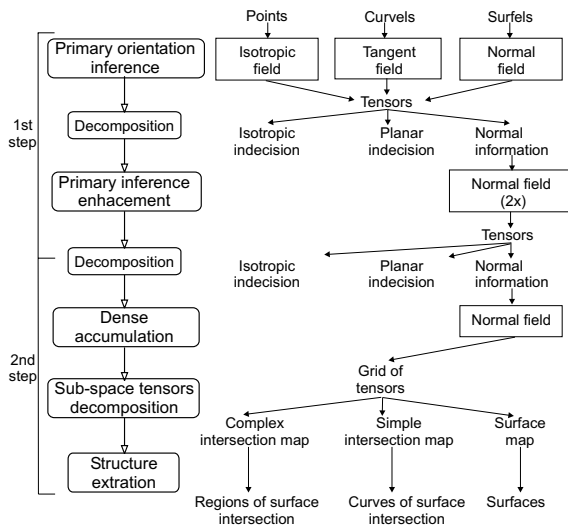


Figure 1: Method overview.

## 3 Accumulation method for finding normals

In the method described in [8], the procedures and mathematical notions originally proposed by Guy are adapted for robust normal inference.

More precisely, we propose new tensorial fields that are treated as surface specific *structuring elements* in an accumulation method. These fields are composed by symmetric second order *orientation tensors* [7]

$$\mathbf{T} = \lambda_1 \mathbf{e}_1 \mathbf{e}_1^T + \lambda_2 \mathbf{e}_2 \mathbf{e}_2^T + \lambda_3 \mathbf{e}_3 \mathbf{e}_3^T, \quad (1)$$

where orientations are coded in eigenvectors  $\mathbf{e}_1 \perp \mathbf{e}_2 \perp \mathbf{e}_3$  with their respective eigenvalues  $\lambda_1 \geq \lambda_2 \geq \lambda_3 \geq 0$  representing pertinences.

Aligned with an input element, a tensorial field defines normal contributions in space. The contributions of every input are then accumulated for normal inference. In our method, the secondary information in resultant tensors is interpreted as indecision of normal estimation [9].

### 3.1 Normal tensorial field

The normal field is the most important in the accumulation method. Its trajectories define the expected curvature for surface reconstruction. We chose the vectorial and force fields with identical connecting trajectories converging to the origin.

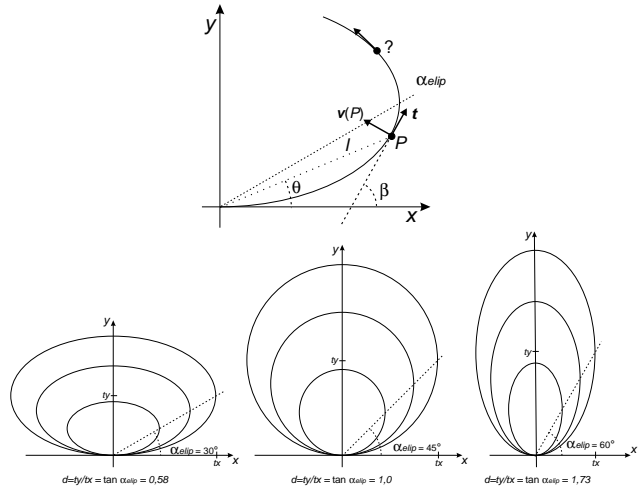


Figure 2: Ellipses with different shapes.

The trajectory curvature may be controlled by using ellipses centered in the  $y$  axis and tangent to the  $x$  axis

$$\frac{x^2}{t_x^2 k^2} + \frac{(-t_y + \frac{y}{k})^2}{t_y^2} = 1 \quad (2)$$

where  $t_x$  and  $t_y$  are constants and  $k$  define the ellipse having axis parallel to  $x$  and to  $y$  with sizes  $2kt_x$  and  $2kt_y$  respectively. The ellipses shape defines the connections curvature

and can be easily controlled by the ratio of axis sizes

$$d = \frac{2kt_y}{2kt_x} = \frac{t_y}{t_x} \quad (3)$$

that is the same for all ellipses of a family. Figure 2 shows some ellipse families with different values of  $d$ . The circular continuity is obtained with  $d = 1$ .

Given a point  $P \in \mathbb{R}^2$  with polar coordinates  $(\rho, \theta)$ , the inclination of the line tangent to the ellipse (Eq. 2) passing by  $P$  is

$$\tan \beta = \frac{2d^2 \tan \theta}{d^2 - \tan^2 \theta}, \quad \cos \theta \neq 0 \text{ and } d \neq |\tan \theta| \quad (4)$$

with  $\beta$  being the angle between this line and  $x$  axis (Fig. 2). When  $|\tan \theta| = d$ , the tangent line is perpendicular to the  $x$  axis ( $\beta = 90^\circ$ ), invalidating Eq. 4. One point cannot be connected to the origin beyond these ellipse extremes. They form the maximal connection angle  $\alpha_{elip}$  (Fig. 2) that defines the ellipse family assigning

$$d = \tan \alpha_{elip}. \quad (5)$$

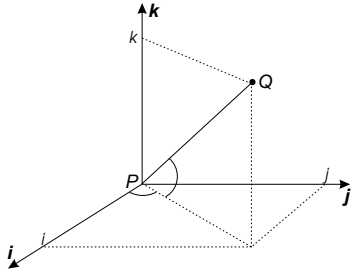


Figure 3: Spherical coordinates of a point  $Q$  in the coordinate system of a surfel  $(P, \mathbf{k})$ .

Consider a surfel  $(P, \mathbf{k}) \in \mathbb{R}^3 \times \mathbb{R}^3$  and the unit vectors  $\mathbf{i} \perp \mathbf{j}$ , all arbitrary but perpendicular to  $\mathbf{k}$ . The normal vector  $\mathbf{k}$  defines the plane  $\mathbf{ij}$  represented by the surfel. The point  $P$  and the orthonormal base  $\{\mathbf{i}, \mathbf{j}, \mathbf{k}\}$  form a coordinate system in  $\mathbb{R}^3$  (Fig. 3). The spherical coordinates  $(\rho, \phi, \theta)$  of a point  $Q \in \mathbb{R}^3$  are:

$$\rho = |PQ|, \quad \tan \phi = \frac{k}{\sqrt{i^2 + j^2}}, \quad \tan \theta = \frac{j}{i}$$

where  $i = \mathbf{i} \cdot PQ$ ,  $j = \mathbf{j} \cdot PQ$  and  $k = \mathbf{k} \cdot PQ$  are the cartesian coordinates of  $Q$  in the system (Fig. 3). Eq. 4 can be used to compute the angle  $\beta$  between the plane  $\mathbf{ij}$  and the tangent plane to the ellipsoid passing by  $Q$ :

$$\tan \beta = \frac{2d^2 \tan \phi}{d^2 - \tan^2 \phi},$$

$$\cos \phi \neq 0, \quad d = \tan \alpha_{elip} \text{ and } d \neq |\tan \phi|$$

where  $\alpha_{elip}$  is the maximal connection angle. The 3D vectorial field for normals is defined by

$$\mathbf{v}_N((P, \mathbf{k}), Q) = (\mathbf{i} \cos \theta + \mathbf{j} \sin \theta) \cos \left( \beta + \frac{\pi}{2} \right) + \mathbf{k} \sin \left( \beta + \frac{\pi}{2} \right) \quad (6)$$

where the addition of  $\pi/2$  to  $\beta$  defines vectors normal to the ellipsoids.

The force gradient field should define the same trajectory of the vectorial field. Thus, the equipotential surfaces of force must be orthogonal trajectories to the ellipsoids. The farthest distance from the origin of the orthogonal trajectory passing by  $Q$  is given by

$$s((P, \mathbf{k}), Q) = \rho \cos \phi \left( 1 + \left( 2 - \frac{1}{d^2} \right) \tan^2 \phi \right) \frac{d^2}{2d^2 - 1}$$

forming the attenuated scalar field

$$f_N((P, \mathbf{k}), Q) = e^{-\frac{s((P, \mathbf{k}), Q)^2}{\sigma^2}}$$

whose gradient vectors define the same trajectories of the vectorial field (Eq. 6). The normal tensorial field defining elliptical connections for a surfel  $(P, \mathbf{k})$  in 3D is

$$C_N((P, \mathbf{k}), Q) = \begin{cases} r\mathbf{v}\mathbf{v}^T, & \text{if } \phi \leq \alpha_{max} \\ \mathbf{0}, & \text{if } \phi > \alpha_{max} \end{cases},$$

$$\alpha_{max} \leq \alpha_{elip}, \quad r = f_N((P, \mathbf{k}), Q), \quad \mathbf{v} = \mathbf{v}_N((P, \mathbf{k}), Q)$$

where  $\alpha_{elip}$  defines the maximal angle and the curvature. The  $\alpha_{max}$  parameter can be used to define fields with smaller influence than  $\alpha_{elip}$ .

### 3.2 Tangent tensorial field

A curvel  $(P, \mathbf{t}) \in \mathbb{R}^3 \times \mathbb{R}^3$  defines a straight line that can be interpreted as an intersection of planes in space. Thus, there is only one plane passing by  $(P, \mathbf{t})$  and a point  $Q$  having normal

$$\mathbf{v}_T((P, \mathbf{t}), Q) = \frac{\mathbf{w}}{|\mathbf{w}|}, \quad \mathbf{w} = \mathbf{t} \times PQ, \quad (7)$$

that represents the vectorial field for curvels.

The force field should be radial and stronger for points near  $P$ :

$$f_I(P, Q) = e^{-\frac{|PQ|^2}{\sigma^2}}, \quad (8)$$

where  $\sigma$  is the attenuation factor. The tangent tensorial field for curvels in 3D is

$$C_T((P, \mathbf{t}), Q) = r\mathbf{v}\mathbf{v}^T, \quad r = f_I(P, Q), \quad \mathbf{v} = \mathbf{v}_T((P, \mathbf{t}), Q).$$

### 3.3 Isotropic tensorial field

A point with no associated orientation  $P \in \mathbb{R}^3$  has insufficient information to induce normals directly on another

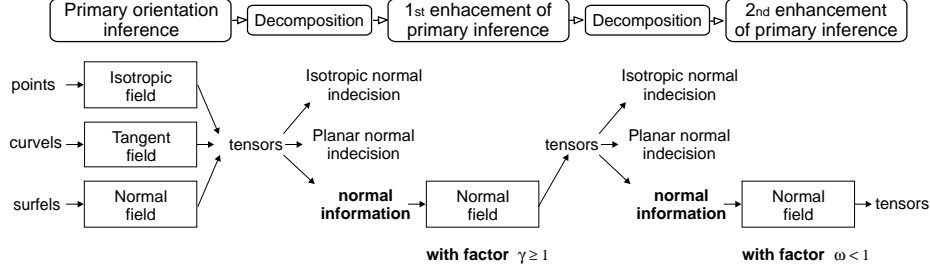


Figure 4: Orientation inference with two enhancing accumulations.

point  $Q$ . Any plane passing by the straight line  $PQ$  is valid. The vectorial field defining this line

$$\mathbf{v}_I(P, Q) = \frac{PQ}{|PQ|}$$

should be used to code this planar indecision for normals.

Using the scalar force of Eq. 8, the isotropic tensorial field in 3D is

$$C_I(P, Q) = r(\mathbf{I} - \mathbf{v}\mathbf{v}^T), \quad r = f_I(P, Q), \quad \mathbf{v} = \mathbf{v}_I(P, Q)$$

where  $\mathbf{I}$  is the identity matrix. The plane estimated to have the normal is coded in  $\mathbf{e}_1\mathbf{e}_2$  with  $\mathbf{e}_3 = \mathbf{v}_I(P, Q)$  (Eq. 1). The force is coded in  $\lambda_1 = \lambda_2 = f_I(P, Q)$  with  $\lambda_3 = 0$ .

### 3.4 Primary orientation inference

The primary inference is performed by the accumulation of influences of all input points. Consider an input set  $D$  composed of  $n = i + j + k$  elements. To infer their orientations, every element of the total input points

$$Q = \{P_1, \dots, P_i\} \cup \{N_1, \dots, N_j\} \cup \{T_1, \dots, T_k\}, \quad (9)$$

has an associated orientation tensor  $\mathbf{T}_m \in \{\mathbf{T}_1, \dots, \mathbf{T}_n\}$  representing the total influence of sparse data

$$\mathbf{T}_m = \sum_i C_I(P_i, Q_m) + \sum_j C_N((N_j, \mathbf{n}_j), Q_m) + \sum_k C_T((T_k, \mathbf{t}_k), Q_m)$$

where  $Q_m$  is the  $m$ -th point of  $Q$ . Every tensor  $\mathbf{T}_m$  contains the inferred orientation for its corresponding point  $Q_m$  from every input elements of  $D$ . This is primary information because the tangent and isotropic tensorial fields do not define smooth surfaces. Besides, noisy elements have the same weight of more precise elements.

### 3.5 Enhancing the primary inference

We propagate the information of normal contained in  $\mathbf{T}_m$  using the normal tensorial field to enhance the primary inference. We argue that:

- the normal field is morphologically adapted to infer normals forming smooth surfaces and balanced pertinences;
- the use of the pertinence obtained in primary inference reduces the effect of less structured elements. We hope that noisy elements have lower pertinence;
- the information repropagation allows an extended evaluation of normal vectors.

The normal information of an orientation tensor  $\mathbf{A} = \lambda_1\mathbf{e}_1\mathbf{e}_1^T + \lambda_2\mathbf{e}_2\mathbf{e}_2^T + \lambda_3\mathbf{e}_3\mathbf{e}_3^T$  is given by functions

$$\mathbf{v}\mathbf{n}(\mathbf{A}) = \mathbf{e}_1, \quad s(\mathbf{A}) = \lambda_1 - \lambda_2$$

where  $\mathbf{v}\mathbf{n}$  is the normal vector and  $s$  is its pertinence.

A new tensor set  $\mathbf{U}_m \in \{\mathbf{U}_1, \dots, \mathbf{U}_n\}$  is associated to the set of input points  $Q$  and defined by the propagation of the normal information contained in  $\mathbf{T}_m$ :

$$\mathbf{U}_m = \sum_{l=1}^n s(\mathbf{T}_l)^\gamma C_N((Q_l, \mathbf{v}\mathbf{n}(\mathbf{T}_l)), Q_m) \quad (10)$$

where  $(Q_l, \mathbf{v}\mathbf{n}(\mathbf{T}_l))$  is the tuple composed by  $n$  input points and their estimated normals.

The factor  $\gamma$  is used for pertinence regularization. If  $\gamma \geq 1$ , the difference among them is amplified. Elements with low pertinence tends to have lower influence, favoring noise filtering. This may generate holes in regions with low point density. If  $\gamma < 1$ , the difference between pertinences is reduced, inducing an influence equalization. In presence of noise, this may disturb reconstruction processes.

For general applications, we suggest propagating normal information twice (Fig. 4). The first time, we estimate  $\mathbf{U}_m$  with  $\gamma \geq 1$  (Eq. 10) to filter the primary orientations. Associating the tensor set  $\mathbf{V}_m \in \{\mathbf{V}_1, \dots, \mathbf{V}_n\}$  to the set of input points  $Q$ , the second normal propagation is given by

$$\mathbf{V}_m = \sum_{l=1}^n s(\mathbf{U}_l)^\omega C_N((Q_l, \mathbf{v}\mathbf{n}(\mathbf{U}_l)), Q_m) \quad (11)$$

where  $\omega < 1$  is the regularization factor. This second accumulation reduces the difference among the pertinences

obtained in  $U_m$ , also reducing the filtering effect in regions with low point density.

Two accumulations were effective to enhance the normal estimation but the process may be modified. Experiments performed show that  $\gamma = 1$  and  $\omega = 1/2$  give good results in general applications.

The orientation inference above evaluates the spatial organization of sparse data in terms of surfaces. It has several applications.

Ideally, the sparse accumulation should assign maximal pertinence to the structured points and minimal to the unorganized. The more precise pertinence values provided by our functions tend to give greater pertinences to the organized points. This bimodal aspect of pertinence distribution enables the use of a threshold for segmenting both sets.

In [10], we propose a method for sparse data filtering suitable for preprocessing purposes. In [11], we show the use of this filtering method in altimetry data to find vegetation regions.

#### 4 Accumulation process for reconstruction

For surface reconstruction, the normal tensorial field is used to propagate the normal information obtained for each input element into subspace containing all elements. More precisely, the original surface normals are inferred for every point  $P \in S$  of a subspace  $S \subset \mathbb{R}^3$  containing the input set  $D$  by the following accumulation function:

$$I(D, P) = \sum_{l=1}^n s(\mathbf{V}_l) C_N((Q_l, \mathbf{vn}(\mathbf{V}_l)), P)$$

where  $Q_l$  is the  $l$ -th input point (Eq. 9) and  $\mathbf{V}_l$  is its orientation tensor obtained in enhanced inference (Eq. 11).

Actually, subspace  $S$  is represented by a discrete grid of tensors  $\mathbf{G}_{i,j,k}$  with dimensions  $r \times t \times u$  with  $i, j, k, r, t, u \in \mathbb{Z}^+$ . Thus, the dense accumulation given the subset  $D$  is defined by

$$\mathbf{G}_{i,j,k} = I(D, H(i, j, k)), \quad i \leq r, \quad j \leq t, \quad k \leq u$$

where function  $H: \mathbb{Z}^{+3} \rightarrow \mathbb{R}^3$  represents the transformation of discrete coordinates  $(i, j, k)$  in real coordinates corresponding to subspace  $S$ .

##### 4.1 Surface extraction

The discrete grid  $\mathbf{G}_{i,j,k}$  is decomposed in pertinence maps of dimensions  $r \times t \times u$  as defined by Guy:

- surface map:  $s = \lambda_1 - \lambda_2, \mathbf{e} = \mathbf{e}_1$ ;
- simple surface intersection map:  $s = \lambda_2 - \lambda_3, \mathbf{e} = \mathbf{e}_3$ . In best case, the planar indecision of normals indicates intersection of planes forming curves;

- complex surface intersection map:  $s = \lambda_3, \mathbf{e} = \mathbf{0}$ . Isotropic indecision reflects absence of dominating normal. High reponses may indicate complex intersections of planes.

The structures are extracted from local maxima in each map. In surface map, a point  $H(i, j, k)$  is over a surface if its pertinence  $s$  is a local maxima in direction of estimated normal vector  $\mathbf{e}$ . Guy defined a variation of marching cubes algorithm to extract these localities as closed surfaces.

The extraction of curves and closed regions from intersection maps may give surface intersections. However, high reponses of pertinence in these maps may indicate noise presence. Thus, their names are merely suggestive.

## 5 Experimental results

We present qualitative and quantitative experiments to put in evidence the key differences between the original methods and ours. Qualitative results allow the evaluation of reconstruction visual quality. In other hand, quantitative experiments show the evolution of precision evaluations for comparing all methods.

### 5.1 Qualitative results

The parameters of each method were adjusted by comparison of several results. For our method, we used  $\gamma = 1$  (Eq. 10) and  $\omega = 1/2$  (Eq. 11). Reconstructions with circular continuity  $\alpha_{elip} = 45^\circ$ , and elliptic  $\alpha_{elip} = 60^\circ$  are given. Both with maximal angle  $\alpha_{max} = 45^\circ$  (Eq. 7).

For Guy's method, we set  $a = 3$  and  $b = 1$  to define a normalized force field between  $-1 \leq x \leq 1$ . Lee & Medioni method is applied with  $c = 0.02$ . See [5] for a complete description of these methods.

Fields should have finite extensions for performance issues. The force may be considered null beyond a distance  $dmax$  from field's central point. To have coherent results, the force field parameters of all methods are adjusted in such a way that

$$f(P, Q) \leq k \quad \forall Q \in \mathbb{R}^3 \mid |PQ| \geq dmax \quad (12)$$

where  $P$  is the field's central point. Every point at distance  $dmax$  can have  $k$  as maximum force. In anisotropic fields, the most aligned points have force  $k$ .

Fig. 5 shows 250 points forming a Cassini's oval with 1500 outliers uniformly distributed in the cube of side 15% greater than the cube containing the oval. The two tori of Fig. 6 are composed by 2000 points with tangents forming rings. The topology is complex and several approaches fail in reconstructing it. Both models were used in the original methods.

For Cassini's oval, we used  $dmax = 0.22$  for ours and Guy methods and  $dmax = 0.21$  for Lee's one. All

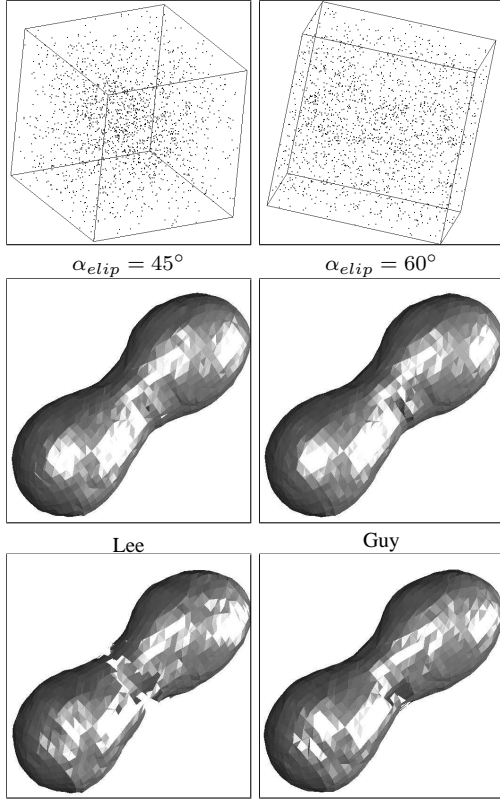


Figure 5: Reconstruction of Cassini's oval in a grid of dimensions  $50 \times 50 \times 50$ .

methods extracted the object (Fig. 5) but only our method could reconstruct it entirely as a smooth surface. Note that a smoother surface was obtained with  $\alpha_{elip} = 60^\circ$  due to the elliptic curvature.

For the two tori, we used  $dmax = 0.10$  for our method and  $dmax = 0.11$  for Lee and Guy methods. As with Cassini's oval example, more regular surfaces were obtained with  $\alpha_{elip} = 60^\circ$ .

The cut views of Cassini's oval grid show that our method gives better results with noisy data (Fig. 7). It reduces considerably the pertinences of points not organized over surfaces. This is due to our tensorial fields and the enhancement of the primary normal inference. Note that Lee & Medioni method is the most sensible to noise.

Our method also gives more balanced pertinence distributions over the surfaces. It is showed in the cut views of the two tori (Fig. 7).

## 5.2 Quantitative results

Evaluate the efficiency or precision of reconstruction methods is a hard task. In some situations it is not even possible because of the difficulty in establishing viable criteria.

In our case, all methods are under the same paradigm

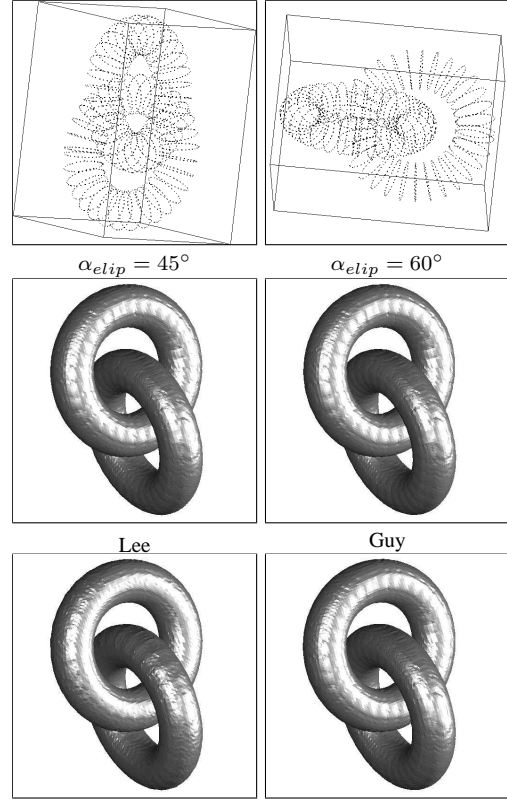


Figure 6: Reconstruction of the two tori in a grid of dimensions  $75 \times 100 \times 75$ .

and their parameters have the same meanings. It simplifies the development of a protocol to evaluate the reconstruction of specific models.

A reconstructed surface  $S$  is composed by  $k$  distinct points  $\{V_1, \dots, V_n\}$  forming triangles. One may estimate the general quality by the *mean squared error*  $\overline{mse}$ :

$$\overline{mse}(S, U) = \frac{1}{k} \sum_{i=1}^k \varepsilon^2, \quad \varepsilon = d(P_i, U) \quad (13)$$

where  $d$  is the smallest euclidian distance between the point  $P_i$  and the original surface  $U$ .

For precise error evaluation, it is necessary a great number  $n$  of samples  $D_i$  obtained in the same conditions and representing independent objects  $M_i$  of the same class. Expected error average for this class is computed by the average of the individual errors of the reconstructions  $S_i$  of  $D_i$ :

$$E(\overline{mse}) = \frac{1}{n} \sum_{i=1}^n \overline{mse}(S_i, M_i). \quad (14)$$

Objects  $M_i$  may have different orientations and shapes but must represent the same structure. Samples should have the same spatial features like density and distribution.

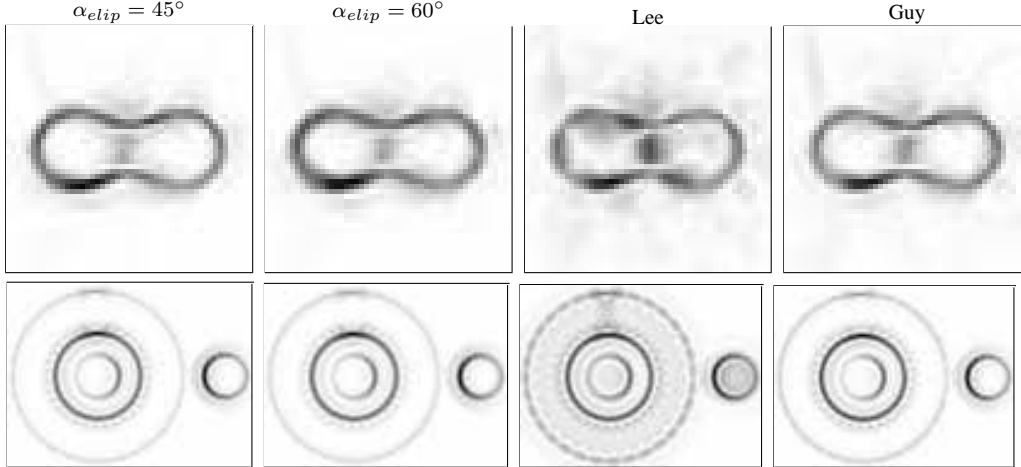


Figure 7: Cut view of the discrete grids illustrating the normalized pertinence of normal inference. Darker points have greater pertinences.

Mean squared error estimates (Eq. 13) are only valid for good approximations of the original object. Note that the closest point of  $P_i$  is not necessarily its homologue in the original surface. Besides,  $S_j$  can be a partial reconstruction of  $M_j$  and still have low average error.

We observed that the number of triangles of invalid reconstructions diverges from the average of all reconstructions. These rare surfaces must be excluded from the expected error calculation (Eq. 14). Thus, we use the average  $\bar{t}$  and standard deviation  $\sigma(t)$  of number of triangles obtained from  $n$  samples

$$\bar{t} = \frac{1}{n} \sum_{i=1}^n t_i, \quad \sigma(t) = \sqrt{\frac{1}{n} \sum_{i=1}^n t_i^2 - \bar{t}^2}, \quad (15)$$

to indicate the range  $\bar{t} \pm b\sigma(t)$  defining valid reconstructions. A surface  $S_j$  is rejected if  $t_j < \bar{t} - b\sigma(t)$  or  $t_j > \bar{t} + b\sigma(t)$ . The adaptative threshold with  $b = 2$  proved to be efficient to exclude invalid reconstructions.

### 5.3 Evaluating ellipsoid reconstruction

Evaluation is made by reconstructing ellipsoids with several shapes and orientations. The goal is to show methods behavior with surfaces having variable curvature.

Every sample is generated by the application of a linear operator on 250 points uniformly distributed over the unit sphere centered at  $(0, 0, 0)$ . These linear operators are symmetric positive matrices. Eigenvalues indicate the size of ellipsoid axis. The greatest eigenvalue is chosen randomly in range  $[1, 1.4]$  and the smallest between  $[0.6, 1]$ . We fix the intermediary eigenvalue in 1. Eigenvectors define the axis orientation and are also determined randomly.

The change of points density caused by the transfor-

mation does not affect the reconstructions. We use a discrete grid of dimensions  $40 \times 40 \times 40$ .

Fig. 8a shows the evolution of error in function of  $dmax$ . High values of  $dmax$  can generate bad surfaces because the increase of cross-talking between distant points. For ellipsoid reconstruction, the high curvature regions get smoother, which explains the average error augmentation.

Our method with  $\alpha_{elip} = 45^\circ$  approximates better the high curvature regions obtaining smaller error estimates. For  $dmax > 0.03$ , the Guy, Lee and  $\alpha_{elip} = 60^\circ$  methods have the same behavior. Note that Lee's method does not give good results with low values of  $dmax$ .

Error evolution with number of outliers varying between 250 and 1000 is showed in Fig. 8b. We used  $dmax = 0.30$  for all methods. Clearly, the dedicated method gave better results due to the primary inference enhancement. Guy and Lee methods have the same behavior until 150% of outliers. Beyond this limit, Lee's method gave better results. With high noise rates, the tangent propagation of Lee's method enforces the location of surfaces.

Fig. 8c shows the error evolution in function of additive noise with normal distribution. We used  $dmax = 0.30$  for all methods. The evolution of Guy and Lee curves indicates that their methods have similar behavior. The displacement of Lee's curve does not mean lower sensibility to noise. Our method presents a smaller evolution of error average. The method with  $\alpha_{elip} = 60^\circ$  gives slightly better results than with  $\alpha_{elip} = 45^\circ$ .

## 6 Conclusions

We have presented a method dedicated to surface reconstruction based on a specific interpretation of tensor orientation, an appropriated construction of tensorial fields and

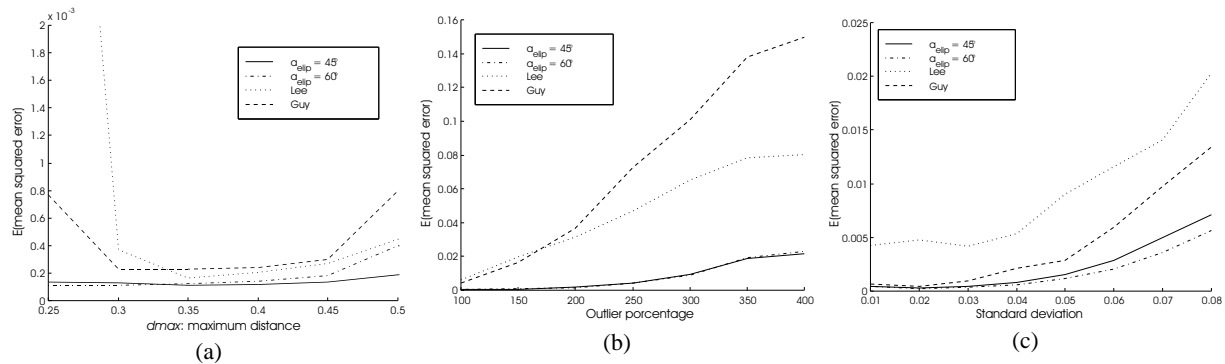


Figure 8: Error evolution for ellipsoid reconstruction. (a) Varying the maximum distance  $d_{\text{max}}$ . Average of 150 samples for each  $d_{\text{max}}$ . (b) Varying the number of outliers. Average of 122 samples for each noise level. (c) Varying the standard-deviation of additive noise. Average of 236 samples for each standard-deviation.

an enhanced normal inference. Our results show that it is less sensible to noise and to parameters variation.

The Cassini’s oval reconstruction and the error evolution varying the number of outliers (Fig. 8b) demonstrate the positive effects of the normal inference enhancement. This process reduces the pertinence of point not structured over surfaces. It explains the good performance of our method with noisy samples. Balanced pertinence estimates are responsible for the lower sensibility of the method to  $d_{\text{max}}$  variations (Fig. 8a).

Elliptic trajectories are proposed to adjust the method to different kinds of sparse data. The reconstruction results of samples with additive noise (Fig. 8b) show that smaller curvature connections are better in this case.

A dedicated method for curve reconstruction can be defined by the same ideas of this research. Also, efficiency may be enhanced by developing new influence fields, iterative processes and heuristics for organization inference.

Further information about our accumulation method and its applications can be found in [8].

## Acknowledgements

The authors are grateful to CAPES/COFECUB and CNPq for the financial support to this work.

## References

- [1] Hugues Hoppe, *Surface Reconstruction from Unorganized Points*, Ph.D. thesis, University of Washington, 1994.
- [2] Nina Amenta, Marshall Bern, and Manolis Kmvyselis, “A new voronoi-based surface reconstruction algorithm,” in *SIGGRAPH*, 1998, pp. 415–421.
- [3] M. Gopi and S. Krishnan, “A fast and efficient projection-based approach for surface reconstruction,” *High Performance Computer Graphics, Multimedia and Visualization*, vol. 1, no. 1, pp. 1–12, 2000.
- [4] Gideon Guy, *Inference of Multiple Curves and Surfaces from Sparse Data*, Ph.D. thesis, IRIS/University of Southern California, 1996.
- [5] Gérard Medioni, Mi-Suen Lee, and Chi-Keung Tang, *A Computational Framework for Segmentation and Grouping*, Elsevier Science B.V., 1 edition, 2000.
- [6] Mi-Suen Lee and Gérard Medioni, “Grouping  $\cdot$ ,  $-$ ,  $\rightarrow$ ,  $0$ , into regions, curves, and junctions,” *IEEE Computer Vision and Image Understanding*, vol. 76, no. 1, pp. 54–69, Oct. 1999.
- [7] Hans Knutsson, “Representing local structure using tensors,” in *The 6th Scandinavian Conference on Image Analysis*, Oulu, Finland, June 1989, pp. 19–22.
- [8] Marcelo Bernardes Vieira, *Orientation Inference of Sparse Data for Surface Reconstruction*, Ph.D. thesis, Universidade Federal de Minas Gerais (Brazil) and Université de Cergy-Pontoise (France), 2002.
- [9] Carl-Fredrik Westin, *A Tensor Framework for Multidimensional Signal Processing*, Ph.D. thesis, Linköping University/Sweden, 1994.
- [10] Marcelo B. Vieira, Matthieu Cord, Paulo P. Martins Jr., Arnaldo de A. Araújo, and SylviePhilipp-Foliguet, “Filtering sparse data with 3d tensorial structuring elements,” in *proceedings of SIBGRAPI*, Fortaleza, Brazil, Oct. 2002.
- [11] Matthieu Cord, Michel Jordan, Thomas Belli, and Marcelo Bernardes Vieira, “Analyse d’images aériennes haute résolution pour la reconstruction de scènes urbaines,” *Société Française de Photogrammétrie et Télédétection*, , no. 166, pp. 34–43, 2002.